International Journal For Advanced Research In Science & Technology
A peer reviewed international journal
www.ijarst.in
ISSN: 2457-0362

Power quality Enhancement of Wind and Battery Storage Systems using Three Phase Inverter

Tadapaneni Aparna[1], Pasupuleti Ankamma Rao[2]
[1]PG Student, Dept of EEE, Amrita Sai Institute of Science and Technology (Autonomous).
[2]Assit Professor, Dept of EEE, Amrita Sai Institute of Science and Technology (Autonomous).
[1]aparnatadapaneni123@gmail.com, [2]ankamaraopasupulety@gmail.com

Abstract— in this paper, a novel configuration of a Three Phase inverter that can integrate solar photovoltaic (PV)-Wind with battery storage in a grid-connected system is proposed. The vigor of the proposed topology lies in a novel, elongated unbalance three-level vector modulation technique that can engender the correct ac voltage under unbalanced dc voltage conditions. This paper presents the Fractional order PID design philosophy of the proposed configuration and the theoretical framework of the proposed modulation technique. An incipient fraction order PID controller for the proposed system is additionally presented in order to control the puissance distribution between the solar PV, battery, and grid, which simultaneously provides maximum power point tracking (MPPT) operation for the solar PV. The efficacy of the proposed methodology is investigated by the simulation of several scenarios, including battery charging and discharging with different calibers of solar irradiation. The proposed methodology and topology is tested on MATLAB/SIMULINK Environment.

Index Terms—Battery storage, solar photovoltaic (PV), space vector modulation (SVM), three-level inverter.

I. Introduction

DUE to the world energy crisis and environmental quandaries caused by conventional power generation, renewable energy sources such as photovoltaic (PV) and wind generation systems are becoming more promising alternatives to supersede conventional generation units for electricity generation [1], [2].Advanced power electronic systems are needed to utilize and develop renewable energy sources. In solar PV or wind energy applications, utilizing maximum power from the source is one of the most consequential functions of the potency electronic systems[3]–[5]. In three-phase applications, two types of potency electronic configurations are commonly used to transfer power from the renewable energy resource to the grid:

Single-stage and double-stage conversion. In the Double-stage conversion for a PV system, the first stage is customarily a dc/dc converter and second stage is a dc/ac inverter. The function of the dc/dc converter is to facilitate the maximum power point tracking (MPPT) of the PV array and to engender the congruous dc voltage for the dc/ac inverter. The function of the inverter is to engender three-phase sinusoidal voltages or currents to transfer the potency to the grid in a grid-connected solar PV system or to the load ina stand-alone system [3]–[5].In the single-stage connection, only one converter is needed to consummate the double-stage functions, and hence the system will have a lower cost and higher efficiency, however, a more intricate control method will be required. The current norm of the industry for high power applications is a three-phase, singlestagePV energy systems by utilizing a voltage-source converter(VSC) for power conversion [4].One of the major concerns of solar and wind energy systems is their capricious and fluctuating nature. Grid-connected renewable energy systems accompanied by battery energy storage can surmount this concern. This withal can increment the flexibility of puissance system control and raise the overall availability of the system [2]. Conventionally, a converter is required to control the charging and discharging of the battery storage system and another converter is required for dc/ac power conversion; thus, a threephasePV system connected to battery storage will require two converters. This paper is concerned with the design and study of a grid-connected three-phase solar PV system integrated with battery storage utilizing only one three-level

International Journal For Advanced Research In Science & Technology
A peer reviewed international journal
www.ijarst.in
ISSN: 2457-0362

converter having the capability of MPPT and ac-side current control, and withal the ability of controlling the battery charging and discharging. This will result in lower cost, better efficiency and incremented flexibility of puissance flow control. The remnant of the paper is organized as follows. Section II describes the structure of a three-level inverter and associated capacitor voltages. Section III presents the proposed topology to integrate solar PV and battery storage and its associated control. Section IV describes the Fractional Order PID Controller Section V describes the simulation and validation of the proposed topology and associated control system. Section VI concludes the paper.

II. STRUCTURE OF A Three PHASE INVERTER

IV. Fractional Order PID Controller

A PID controller is a generic control loop feedback mechanism widely used in industrial control systems. The PID controller attempts to correct the error between a measured process variable and a desired set point by calculating and then outputting a corrective action that can adjust the process accordingly. An integer order PID controller has the following transfer function:

$$G_c(s) = K_p + K_i s^{-1} + K_d s$$

The PID controller calculation (algorithm) involves three separate parameters; the Proportional (K p), the Integral (i K) and Derivative (d K) time-constants. The Proportional gain determines the reaction to the current error, the Integral determines the reaction based on the sum of recent errors and the derivative determines the reaction to the rate at which the error has been changing. The weighted sum of these three actions is used to adjust the process via a control element such as the position of a control valve or the power supply of a heating element. The block diagram of a generic closed loop control system with the PID controller is illustrated in Figure 5.

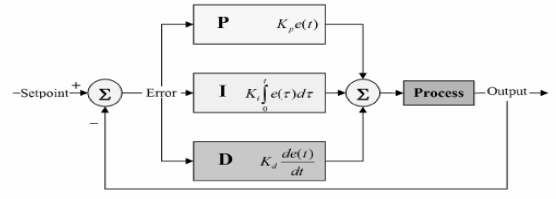

Figure 7. A generic closed-loop process-control system with PID controller

The real objects or processes that we want to control are generally fractional (for example, the voltage-current relation of a semi-infinite lossy RC line). However, for many of them the fractionality is very low. In general, the integer-order approximation of the fractional systems can cause significant differences between mathematical model and real system. The main reason for using integer-order models was the absence of solution methods for fractional-order differential equations. PID controllers belong to dominating industrial controllers and therefore are objects of steady effort for improvements of their quality and robustness. One of the possibilities to improve PID controllers is to use fractional-order controllers with non-integer derivation and integration parts. Following the works of Podlubny [6] we may go for a generalization of the PID-controller, which can be called the PIλD⌈ -controller because of involving an integrator of order and a differentiator of order μ. The continuous transfer function of such a controller has the form:

$$G_c(s) = K_p + T_i s^{-\lambda} + T_d s^{\mu}, (\lambda, \mu > 0)$$

All these classical types of PID-controllers are the special cases of the fractional PIlDμ -controller. As depicted in Figure 2, the fractional order PID controller generalizes the integer order PID controller and expands it from point to plane. This expansion adds more flexibility to controller design and we can control our real world processes more accurately.

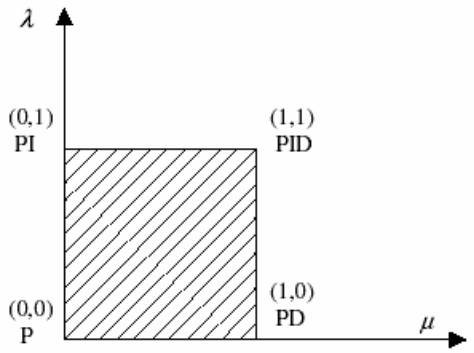

Figure 8. Generalization of the FOPID Controller: From point to plane

V. VALIDATION OF THE PROPOSEDTOPOLOGY AND CONTROL SYSTEM

Simulations have been carried out using MATLAB/Simulinkto verify the effectiveness of the

International Journal For Advanced Research In Science & Technology
A peer reviewed international journal
www.ijarst.in
IJARST
ISSN: 2457-0362

proposed topology and control system. An *LCL* filter is used to connect the inverter to the grid. Fig. 8 shows the block diagram of the simulated system.

TABLE I
PARAMETERS OF THE SIMULATED SYSTEM

V_{BAT}	Vs (line)	L_{BAT}	C_1,C_2	L_l	L_s
60 V	50 V	5 mH	1000 uF	500 uH	900 uH
r_f	C_f	K_p	K_i	G_1	G_2
3 Ω	14 uF	2.9	1700	1	200

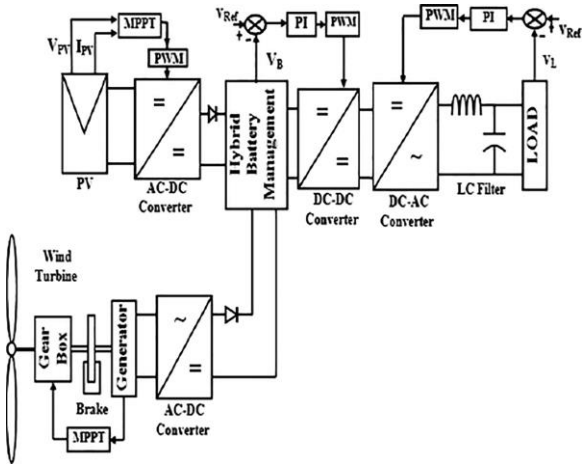

Fig. 8. Block diagram of the simulated system.

Three, series-connected PV modules are used in the simulation. The mathematical model of each of the PV units is given in (21) [21] and used in the simulation where *ISC* is the short circuit current of the PV .In the simulation, it is assumed that *ISC* will change with different irradiances. With a solar irradiation of 1000 W/m2, *ISC*is equal to 6.04 A and the open circuit voltage of the PV panels will be equal to *VoC* = 44V. The main parameters of the simulated system are given in Table I.As discussed in Section III-B, *G*2 must be much more than*G*1 in order to achieve the MPPT condition and to have the flexibility to charge and discharge of the battery. Based on our experiments, any value more than 100 is suitable for this ratio .On the other hand, because the ratio of *G*2 /*G*1 will only affect the short-vector selection, increasing this ratio will not affect other results. This value has been selected to be 200 to have good control on *Vdc* , as shown in Table I. The role of *L*BAT is to smooth the battery current, especially in the transient condition. A wide range of values are acceptable for the inductor value, however, decreasing its value will increase the current overshoot of the battery. Also, its value is dependent of its adjacent capacitor value and its transient voltages. Due to the practical considerations (such as size and cost), the value of *L*BAT is preferred to be low and has been chosen to be 5 mH based our simulation studies. The values of *Kp* and *Ki* are selected by modeling the system in the *dq*-frame. The current control loop can be converted to a simple system after using the decoupling technique shown in Fig 7. The details of this method can be found in [22].For theoretical purposes, two different scenarios have been simulated to investigate the effectiveness of the proposed topology and the control algorithm using a step change in the reference inputs under the following conditions:

1) The effect of a step change in the requested active underactive power to be transferred to the grid when the solar
irradiance is assumed to be constant.

2) The effect of a step change of the solar irradiation when the requested active and reactive power to be transmitted
to the grid is assumed to be constant. In a practical system, a slope controlled change in the reference input is usually used rather than a step change to reduce the risk of mathematical internal calculation errors when working with a limited precision microprocessor system and also to prevent the protection system activation. Furthermore, in practical situations, the inputs of the systems normally do not change instantaneously as a step change, such as the sun irradiation. With this practical application in mind, the proposed system is simulated using a slope controlled change in the requested active power to be transferred to the grid when the solar irradiance is assumed to be constant. To validate this, a laboratory test is carried out using the same scenario and the experimental results given in Section V can be compared with the results from thesimulation.

VI. MATLAB Simulink Result and discussion

The standalone PV system generates electrical energy from the different

International Journal For Advanced Research In Science & Technology
A peer reviewed international journal
www.ijarst.in
ISSN: 2457-0362

irradiance of the Sun. To maximize the operating voltage 34 no's of solar panel is connected in series, which can deliver 14.79 kW power at maximum irradiance condition. To increase reliability of the supplied electricity, battery banks are attached to the system. To the capacity of the supplied electricity without increasing the size of the battery bank, WECS is also attached to the system as a secondary source of energy. The WECS generates electrical energy from the wind and the battery unit stores the generated electrical energy and supplied to the consumer when the primary energy sources are unable to deliver required electrical energy. A three phase rectifier is attached to the PMSM to rectify variable frequency electricity. The generated electricity from the PV and the Wind then connected to a battery unit individually using a charge controller, which maintains the charging, discharging and floating condition and also provides protection of the battery bank. The charge controller also maintains the system as a single battery unit and connected to the PI controlled DC to DC converter. To increase the voltage of the battery a FOPID controlled boost converter is attached to the system. The voltage boost up is necessary to maintain the inverter input voltage constant which helps the inverter control system to maintain the load voltage as desired value. The inverter is connected to the boost DC-DC converter which converts DC to three phase AC with the desired quality using a simple LC filter. To study the overall system performance a variable solar irradiance (Irr), wind speed (Sw) and variable load (PL1 = 16 kW, 0.95 pf, PL2 = 16 kW, 0.9 pf, PL3 = 16 kW, 0.85pf) is applied in this present study and analyse the effectively of the proposed hybrid model which is indicated in Table 1. The Table 1 indicates profile of the variable solar irradiance (Irr), variable wind speed (Sw) and variable load with respect to time. Fig. 9 indicates the performance of the PV array based on the variation of solar irradiance. Fig. 9(a) indicates the profile of the generated current, Fig 9(b) indicates the profile of the generated voltage, Fig. 9(c) indicates the profile of the generated power by the PV array. At the initial condition the IC based MPPT controller performance is slow. The controller takes around 1.6 s to reach the maximum power around 10 kW due to 0.698 kW/m2 solar irradiance. At 2.52 s the irradiance changes to the 0.928 kW/m2 and the PV array generates 13.9 kW. After 4.52 s the irradiance changes to 0.378 kW/m2 and the PV array generates 5.8 kW electricity. In this proposed system a PMSG is attached to the wind turbine to generate electrical energy from the wind. Fig. 10 indicates the performance of the PMSG under variable wind speed. Fig. 10(a) indicates the instantaneous voltage profile of the PMSG and Fig. 10(b) indicates the instantaneous current profile of the generated current generated by the PMSG. The voltage quantity of the PMSG almost constant only the current quantity changes with the change in wind speed.

Table 1
Variation of solar irradiance and wind speed used in this study.

Time (s)	0–2.52	2.52–4.52	4.52–6.00
I_{rr} (kW/m^2)	0.698	0.928	0.378
Time (s)	0–1.69	1.69–4.00	4.00–6.00
S_w (m/s)	10.32	8.00	11.49
Time	0–3	3–5	5–6
Connected Load (kW)	P_{L1}	P_{L1}, P_{L2}, P_{L3}	P_{L1}, P_{L2}

International Journal For Advanced Research In Science & Technology
A peer reviewed international journal
www.ijarst.in
ISSN: 2457-0362

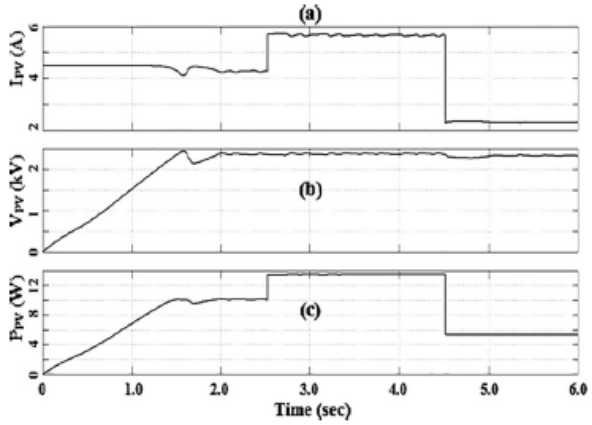

Fig. 9. Generated (a) voltage (b) current (c) power profile of the PV array under variable irradiance of the Sun.

Fig. 11 indicates the performance of the rectifier connected to the PMSG. The generated electrical energy by the PMSG is variable frequency in nature. Hence a rectifier unit is necessary to supply the generated energy to the battery. Fig. 11(a) indicates the profile

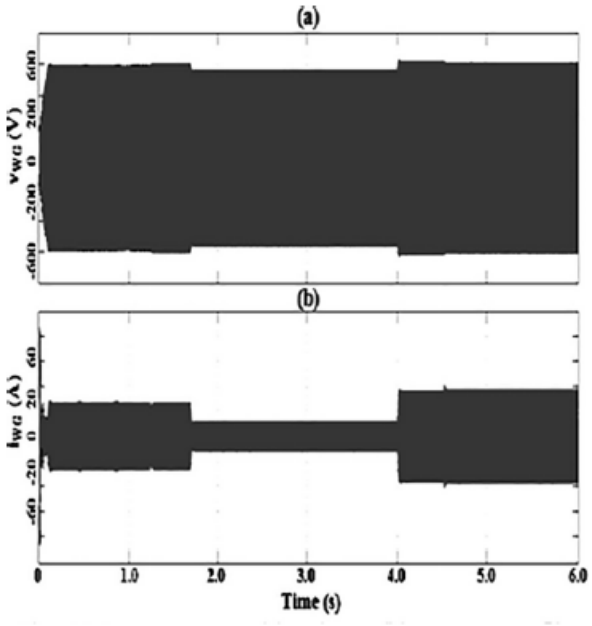

Fig. 10. Instantaneous (a) voltage (b) current profile of the PMSG connected with WT.

of the rectified voltage, Fig. 12(b) indicates the profile of the rectified current, Fig. 12(c) is indicates the profile of the rectified power output due to variable wind speed. Except the initial time the OTC based MPPT controller performance will satisfactory. At the initial condition the PMSG generates power around 13.5 kW due to 10.32 m/s wind speed. At 1.69 s the wind speed reduced to 8 m/s and the PMSG generates 5.3 kW. After 4 s the wind speed changes to 11.49 m/s and the PMSG generates 17 kW. Fig. 13(a) indicates the generated power from the PV array under variable solar irradiance, Fig. 13(b) indicates the generated power by the WTG set under variable wind speed, Fig. 13(c) indicates the comparison of generating power as well as consumed power.

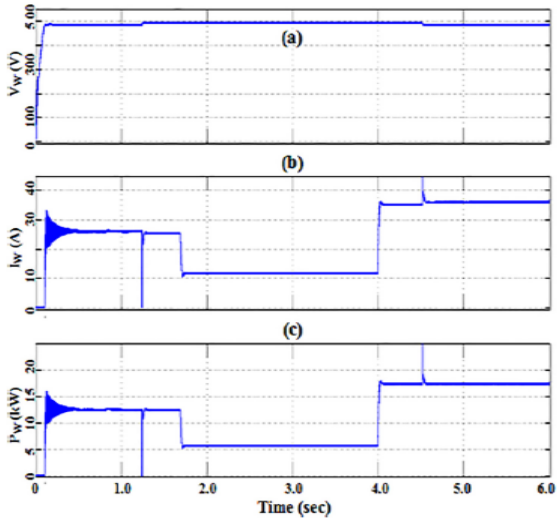

Fig. 11. The rectified (a) voltage (b) current (c) power profile of the PMSG connected with WT.

International Journal For Advanced Research In Science & Technology
A peer reviewed international journal
www.ijarst.in
IJARST
ISSN: 2457-0362

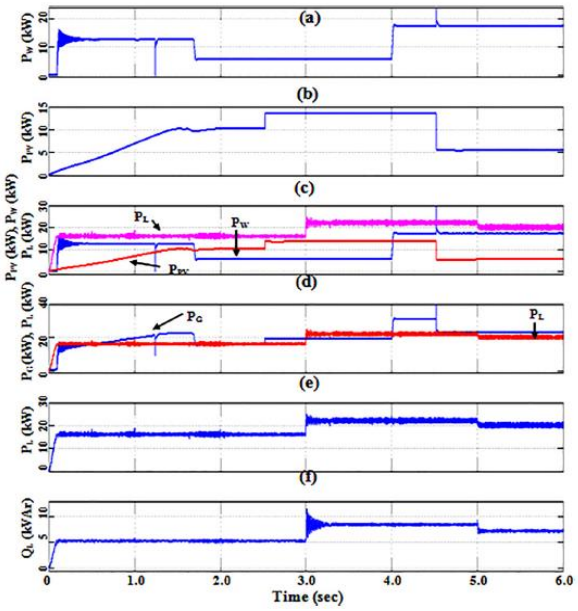

Fig. 12. Generated and connected load profile (a) power generated by WTG (Pw) (b) power generated by PV array (PPV) (c) comparison of generated power and consumed
power (d) comparison of total generated power (PG) and consumed power (PL) (e) active power profile of the load (f) reactive power profile of the load.

Fig. 13(d) indicates the comparison of total generated power by the PV and WTG and the power consumed by the load. Fig. 13(e) and (f) indicates the active and reactive power profile of the load. From Fig. 14(c) it is evident that the generated power by the PV array (PPV) and the generated power by the PMSG (PW) are low compared to the consumed load power (PL). Fig. 13(d) indicates that the total generated power (PG) is comparable with the Load power (PL). Whenever the generated power PG is low compared to the load power PL the battery is in discharging mode, and whenever the generated power PG is more compared to the load power PL the battery is in charging mode. If the generated power (PG) and the consumed power (PL) are equal, the battery is in floating condition. Fig. 11 indicates the load voltage profile under variable load condition. Fig. 11(a) indicates the instantaneous three phase voltage profile which is constant for steady as well as load variation except for the small initial and switching condition of the connected load. Fig. 11(b) clearly indicates the increments and decrement of the load as the instantaneous three phase load current profile changes dependent upon the load demand. Fig. 11(c) indicates the RMS voltage per phase, which is constant for all the simulation time and Fig. 11(d), indicates the line current per phase. Depending upon the load variation the current quantity changes, but the phase voltage is constant for the entire simulation time. To clarify the instantaneous voltage and current profile during the change in load Fig. 11 is enlarged during the change in load and indicated in Fig. 12. Here Fig. 12(a) indicates the instantaneous three phase voltage profile; Fig. 12(b) indicates the instantaneous three phase load current profile. At the initial time the voltage gradually increases and stabilizes at 230 V per phase within 0.095 sec. The current quantity also changes within 0.095 s and stabilized at around 24.3 A per phase. From the Fig. 6.15 it is observed that the time of insertion of the load L2 and L3 the load voltage is constant during the change in load, but the per phase

International Journal For Advanced Research In Science & Technology
A peer reviewed international journal
www.ijarst.in
IJARST
ISSN: 2457-0362

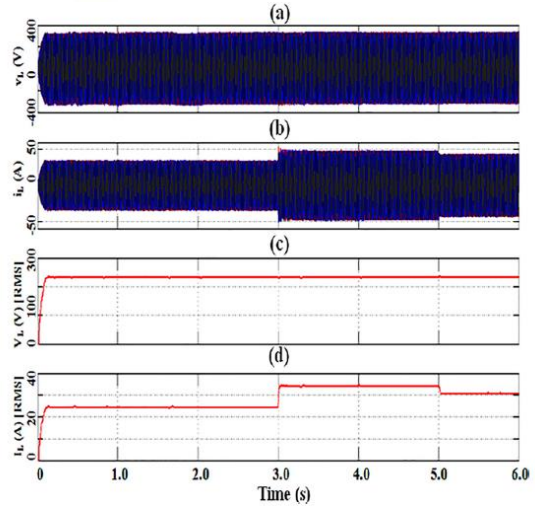

Fig. 13. Dynamic response of dc-ac converter with variable load (a) instantaneous voltage (b) instantaneous current (c) RMS voltage (d) RMS current profile.

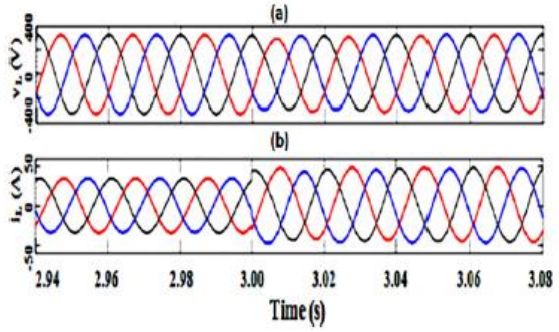

Fig. 14. Dynamic response of dc-ac converter with load increase (a) instantaneous voltage, (b) instantaneous current.

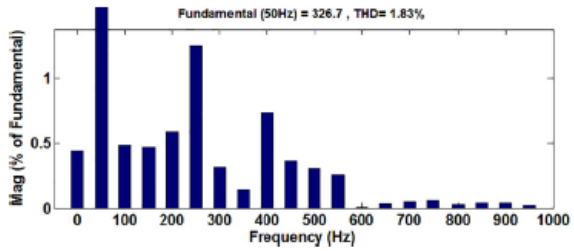

Fig. 15. Harmonic spectrum of load voltage.

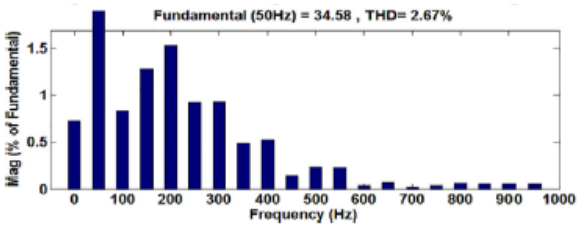

Fig. 16. Harmonic spectrum of load current.

current changes within 0.015 s and stabilizes to around 34 A during maximum load condition. After analysing the Fig. 6.16 it is clearly stated that during the exclusion of L3 load the voltage is stable and the current profile stabilizes within 0.025 s and drawing 30.08 A constant current. Figs. 15 and 16 indicate the harmonic spectrum of load voltage and current. In the proposed system the total harmonic distortion (THD) is around 1.93% for the voltage profile and 1.83% for the current profile which is very much lower as per IEEE 512-1992 standard. In the proposed system, as the quality power is obtained by using simple LC filter which minimize the overall system cost and increase the acceptability of the proposed system.

VI Conclusions

A Standalone hybrid PV–wind-battery-based power evacuation scheme for household application is proposed. The proposed hybrid system provides an elegant integration of PV and wind source to extract maximum energy from the two sources. It is realized by bidirectional dc–dc converter followed by a conventional three phase inverter. A New FOPID control strategy which achieves a better utilization of PV,

wind power, battery capacities without effecting life of battery, and power flow management in stand alone hybrid PV–wind-battery-basedsystem feeding ac loads is presented. Detailed simulation studies are carried out to ascertain the viability of the scheme. The MATLAB simulation results obtained are in close agreement with simulations and are supportive in demonstrating the capability of the system to operate in grid stand-alone mode. The proposed configuration is capable of supplying uninterruptible power to ac loads, and ensures the evacuation of surplus PV and wind power into the Load.

References

1. Arifujjaman, M., 2010. Modeling, simulation and control of load connected Permanent Magnet Generator (PMG)-based small wind energy conversion system. IEEE Electr. Power Energy Conf. 2010, 1–6.
2. Commercial Solar Panels E20-435-COM. https://us.sunpower.com/sites/.../data.../ ds-e20-series-435-commercial-solar-panels.pdf. (Accessed 13 November 2017).
3. Ebrahimi, M.J., 2015. General overview of maximum power point tracking methods for photovoltaic power generation systems. Int. Power Syst. Conf., 136–141 Generic model of a battery. https://in.mathworks.com/help/physmod /sps/
4. powersys/ref/battery.html?s_tid=gn_loc _drop. (Accessed 03 October 2017). Hur, S., 2018. Modelling and control of a wind turbine and farm. Energy 156, 360– 370.
5. Jamal, T., Urmee, T., Calais, M., Shafiullah, G.M., Carter, C., 2017. Technical challenges of PV deployment into remote Australian electricity networks: a review. Renew. Sustain. Energy Rev. 77, 1309–1325.
6. Jena, D., Rajendran, S., 2015. A review of estimation of effective wind speed based control of wind turbines. Renew. Sustain. Energy Rev. 43, 1046–1062.
7. Kamran, M., Mudassar, M., Fazal, M.R., Asghar, M.U., Bilal, M., Asghar, R., mran et al. 2018. Implementation of improved Perturb & Observe MPPT technique with confined search space for standalone photovoltaic system. J. King Saud Univ. – Eng. Sci.
8. Lee, K.J., Lee, J., Shin, D., Yoo, D., Kim, H., 2014. A novel load synchronization PLL method based on adaptive low-pass notch filter for load-connected PCS. IEEE Trans. Industr. Electr. 61 (1), 292–301.
9. Michal, V., 2016. Three-Level PWM floating H-Bridge Sine wave power inverter for high-voltage and high-efficiency applications. IEEE Trans. Power Electr. 31 (6), 4065–4074.
10. Panwar, N.L., Kaushik, S.C., Kothari, S., 2011. Role of renewable energy sources in environmental protection: a review. Renew. Sustain. Energy Rev. 15 (3), 1513– 1524.
11. Rashid, M.H., 2007. Power Electronics Handbook. Elsevier, USA. Saw, L.H., Somasundaram, K.K., Ye, Y., Tay, A.A.O., 2014. Electro-thermal analysis of Lithium Iron Phosphate battery for electric vehicles. J. Power Sources 249, 231– 238.
12. Taleb, M., 2004. Optimal operation of a wind driven system. J. King Saud Univ. – Eng. Sci. 16 (2), 229–251. Tran, Q., Truong, A.V., Le, P.M., 2016. Reduction of harmonics in load-connected inverters using variable switching frequency. Int. J. Electr. Power Energy Syst. 82, 242–251.
13. Wu, Z., Dou, X., Chu, J., Hu, M., 2013. Operation and control of a direct-driven PMSGbased wind turbine system with

an auxiliary parallel load-side converter. Energies 6, 3405–3421.
14. Xiaodong, W., Shixu, H., Shirong, W., Yingming, L., Lixia, L., 2013. Multi-objective optimization torque control of wind turbine based on LQG optimal control. 25th Chinese Control Decision Conf. (CCDC), 405–408.
15. Zammit, D., Staines, C.S., Micallef, A., Maurice, A., Lieari, J., 2017. Incremental current based MPPT for a PMSG micro wind turbine in a load-connected DC microload. Energy Procedia. 142, 2284–2294.
16. Zhihui, Ren, Zhongdong, Yin, Bao, W., 2009. Control Strategy and Simulation of Permanent Magnet Synchronous wind Power Generator. Environment Technology, pp. 568–571.
17. Zoua, C., Zhao, Q., Zhang, G., Xiong, B., 2016. Energy revolution: from a fossil energy era to a new energy era. Natl. Gas Industry B. 3 (1), 1–11.